Performance assessment of a tightly baffled, long-legged divertor configuration in TCV with SOLPS-ITER simulations

G. Sun, H. Reimerdes, C. Theiler, C. Colandrea, B. P. Duval, O. Février, the EUROfusion MST1 team[1] and the TCV team[2]

Ecole Polytechnique Fédérale de Lausanne (EPFL), Swiss Plasma Center (SPC), CH-1015 Lausanne, Switzerland

1. Introduction

In future high power magnetic fusion devices such as DEMO, unmitigated target heat fluxes will greatly exceed material limits. This has motivated the study of a range of innovative divertor designs including radially extended divertor legs, higher-order magnetic nulls, the use of secondary X-points, and improved divertor closure. Some recent concepts of long-legged divertor configurations, such as the long vertical leg divertor proposed by Umansky et al, were predicted to access a passively stable, fully detached, divertor plasma regime from UEDGE code simulations in the ADX tokamak design [1, 2].

The SOLPS-ITER code package is employed, herein, to explore the performance of a tightly baffled, long-legged (TBLL), divertor geometry, which is proposed as a potential divertor concept for validation in TCV. The TBLL divertor will be compared to an unbaffled divertor and one equipped with the existing short inner and longer outer (SI-LO) baffles [3] for plasmas with intrinsic carbon and injected nitrogen impurities. Power handling capabilities and operational limits for core compatibility for nitrogen-seeded detachment are the key parameters assessed in the present work, organized as follows. Section 2 introduces the simulation model with simulation results including target profiles, a range of input powers, and core impurity concentrations presented in Section 3, followed by concluding remarks in Section 4.

2. Simulation setup

The SOLPS-ITER package is a 2D transport code that simulates the scrape-off layer (SOL) plasma by combining the Monte-Carlo neutral transport kinetic code EIRENE and the multi-fluid plasma transport code B2.5.[4] It is widely used to predict and interpret divertor performance for a range of magnetic fusion devices and plasma conditions. Herein, three divertor geometries, shown in Fig. 1 (a)-(c), are simulated based on the TCV shot #64536 that features a lower single null divertor geometry, a magnetic field of 1.4 T and a plasma current

[1] See the author list of B. Labit et al. Nuclear Fusion 59 086020 (2019)
[2] See the author list of H. Reimerdes et al. Nuclear Fusion 62 042018 (2022)

of 250 kA. The radial extent of the modeled grids is limited by the divertor closure as the B2.5 grid can't intercept solid objects other than the target plates, Fig. 1(d, e).

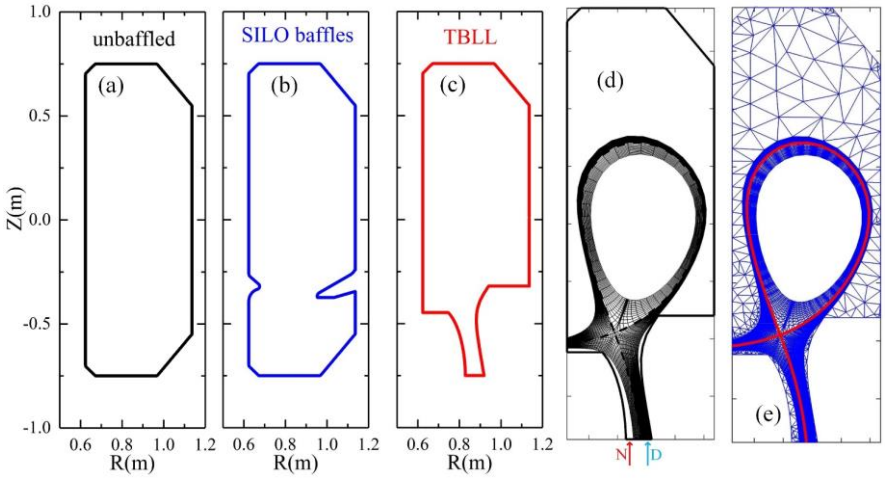

Fig.1. (a)-(c) Geometry of unbaffled, baffled, and TBLL divertor. (d)-(e) Plasma and neutral grid of TBLL divertor. Seeding and fueling locations are indicated, d).

The considered plasma species in the simulations are deuterium, carbon impurities sputtered from the targets and seeded nitrogen impurities. Considering the short dissociation mean free path of molecular nitrogen, nitrogen seeding is, for simplicity, assumed to occur in the form of atomic nitrogen and ammonia formation is neglected. Considered reactions include ionization, charge exchange, dissociation, recombination, elastic collisions and excitation. The outer midplane separatrix density is fixed at $n_{e,sep} = 1.5 \times 10^{19}$ m^{-3} throughout the work, by appropriate adjustment of the deuterium fueling rate and nitrogen seeding rate for each divertor geometry. Fueling rate generally decreases with higher seeding rate but increases with increased divertor closure, for the same upstream density. Recycling coefficients are set to 0.99 for deuterium, 0 for carbon, 1 for neutral and 0.3 for nitrogen ions with a carbon chemical sputtering yield of 3.5%. Unique radial transport coefficients are set at $D_\perp = 0.2\ m^2 s^{-1}$ and $\chi_{\perp,e} = \chi_{\perp,i} = 1.0\ m^2 s^{-1}$. These values are based on previous simulations of Ohmically-heated TCV plasma discharges that were matched to experimental measurements such as Thomson scattering and divertor spectroscopy [5, 6]. Although obtained from L-mode discharges, these values were also used for simulations with high input power to provide qualitative predictions for H-mode operation of the proposed divertors.

3. Simulation results

Higher divertor closure was previously shown to increase the target densities while decreasing the target temperatures T_{ot} and heat fluxes q_{ot} [6]. The TBLL divertor divertor closure is higher than with existing TCV baffles, leading to lower T_{ot} and q_{ot} than, for example, the SILO-baffled divertor, Fig. 2 (a, b). With 800kW entering from the core boundary, the peak

target temperature $T_{ot,max}$ is approximately 50eV without baffles, ~ 10eV with SILO baffles, and well below 5eV (characteristic for the onset of detachment) for the TBLL divertor. This divertor configuration also shows the lowest target heat flux density and highest peak target density (not shown) of the three divertor geometries.

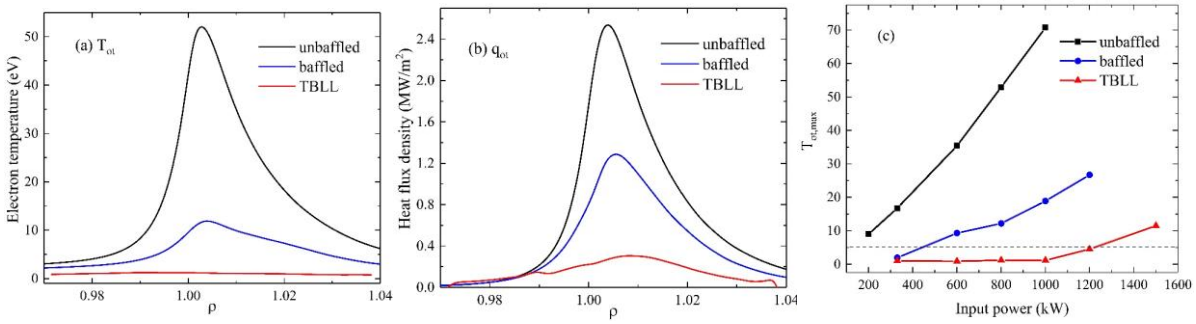

Fig. 2. (a)-(b) Outer target temperature and heat flux density with 800kW input power and no nitrogen seeding. (c) Dependence of $T_{ot,max}$ on heating power. The dashed line indicates the detachment threshold.

A scan of heating power across the core boundary was used to evaluate the power handling capabilities of all three divertors, Fig. 2(c). The detachment threshold of the TBLL divertor is close to 1.2MW that is over two times higher than for the baffled divertor. Heat balance analyses at the outer divertor attribute this increase in the power handling capability of the TBLL divertor to stronger plasma-neutral interaction and impurity radiation than the baffled and unbaffled divertors (not shown). A similar increase of the power handling capability of the TBLL divertor was predicted by the UEDGE simulations in the ARC reactor concept [7].

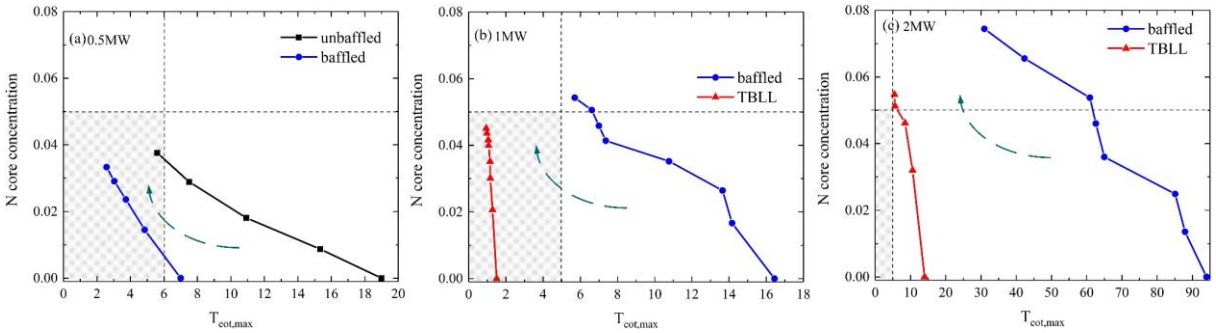

Fig. 3. Core concentration as a function of peak outer target temperature for a scan of seeding rate with input power of (a) 0.5MW, (b) 1MW, (c) 2MW. The arrow direction marks the increasing seeding rate and the operational window marked by the shaded area.

To achieve detachment at higher power levels, nitrogen seeding, increases SOL radiation, is commonly adopted in TCV. Excessive core impurity concentrations, however, lead to core performance degradation or even full plasma radiative collapse. The operational window for detachment is determined by $T_{ot,max} \leq 5\text{eV}$ and an average core nitrogen concentration $\langle C_N \rangle_{core} \leq 5\%$, with the total nitrogen density normalized to the electron density, $C_N =$

$\frac{\sum_{i=0}^{7} n_{N+i}}{n_e}$. A nitrogen seeding rate scan is performed for all divertor configurations for a range of input power levels, Fig. 3. The baffled divertor lies within the operational window with 0.5 MW input power but not at 1MW. The TBLL divertor remains fully within the window for all seeding rates at 1MW and still has a detached operating solution at 2MW. Its operational window with nitrogen seeding is more than twice as wide as that of the baffled divertors.

4. Conclusions

The performance of a proposed implementation of a tightly baffled, long-legged divertor in TCV is evaluated through a comparison with the unbaffled and baffled TCV divertor configurations using SOLPS-ITER simulations. The TBLL divertor is predicted to strongly reduce the target temperature and heat fluxes, with over two times higher power handling capability over the SI-LO baffle configuration. The TBLL divertor also features a much wider operational window for detachment with nitrogen seeding. Together, these results indicate that such a TCV divertor would provide a proof-of-principle of the TBLL divertor concept.

Acknowledgements

This work has been carried out within the framework of the EUROfusion Consortium, funded by the European Union via the Euratom Research and Training Programme (Grant Agreement No 101052200 — EUROfusion). Views and opinions expressed are however those of the author(s) only and do not necessarily reflect those of the European Union or the European Commission. Neither the European Union nor the European Commission can be held responsible for them. This work was supported in part by the Swiss National Science Foundation.

References

1. M. V. Umansky, et al., Nuclear Fusion **60** (1), 016004 (2019).
2. M. V. Umansky, et al., Physics of Plasmas **24** (5), 056112 (2017).
3. H. Reimerdes, et al., Nuclear Fusion **62** (4), 042018 (2022).
4. S. Wiesen, et al., Journal of Nuclear Materials **463**, 480-484 (2015).
5. A. Smolders, et al., Plasma Physics and Controlled Fusion **62** (12), 125006 (2020).
6. M. Wensing, et al., Plasma Physics and Controlled Fusion **61** (8), 085029 (2019).
7. M. R. K. Wigram, et al., Nuclear Fusion **59** (10), 106052 (2019).